J Fluoresc (2015) 25:433–440
DOI 10.1007/s10895-015-1530-4

ORIGINAL PAPER

Nanospherical Silica as Luminescent Markers Obtained by Sol–Gel

Caroline B. Azevedo · TúlioM. Batista · Emerson H. de Faria · Lucas A. Rocha · Katia J. Ciuffi · Eduardo J. Nassar

Received: 12 August 2014 / Accepted: 2 January 2015 / Published online: 17 February 2015

Abstract Hybrid nanosilicas constitute a broad study field. They find application as catalysts, pigments, drug delivery systems, and biomaterials, among others, and it is possible to obtain them via the sol–gel methodology. Lanthanide ions present special properties like light emission. Their incorporation into a silica matrix can enhance their luminescent properties, which enables their application as luminescent markers. This work reports on (i) the preparation of luminescent spherical hybrid silica nanoparticles by the hydrolytic sol–gel methodology, (ii) doping of the resulting matrix with the europium(III) ion or its complex with 1,10-phenanthroline, and (iii) characterization of the final powders by scanning electron microscopy, infrared spectroscopy, X-ray diffraction, and europium(III) ion photoluminescence. The synthesized materials consisted of hybrid, amorphous, polydispersed nonspherical silicas with average size of 180 nm. Photoluminescence confirmed incorporation of the europium(III) ion and its complex into the silica matrix—the ligand-metal charge transfer band emerged in the excitation spectra. The emission spectra presented the bands corresponding to the transition of the excited state $^5D_0$ level to ^7F_J (J = 0, 1, 2, 3 and 4). The main emission occurred in the red region; the lifetime was long. These characteristics indicated that the prepared nanospherical hybrid silicas could act as luminescent markers.

Keywords Europium III complex · Sol–gel · Luminescent

C. B. Azevedo · T. Batista · E. H. de Faria · L. A. Rocha · K. J. Ciuffi · E. J. Nassar (✉)
Universidade de Franca, Av. Dr. Armando Salles Oliveira, 201 Pq. Universitário, Franca, SP CEP 14404-600, Brazil
e-mail: eduardo.nassar@unifran.edu.br

Introduction

In the last 25 years, several works in the field of materials chemistry have dealt with multifunctional hybrid materials for application as catalysts, pigments, drug delivery systems, and biomaterials, as well as for use in the areas of environmental, biological, and medical science [1–5].

The development of nanotechnology has relied mainly on hybrid silicas obtained from organically modified silicates. These materials display properties that make them potentially applicable in photonic devices, thermal insulators, cosmetics, immunoassays, and medical diagnosis, among other fields [6, 7]. These hybrids can be obtained in three different ways: (i) addition of the organic component together with the inorganic component in the liquid phase during the sol–gel process, without a bond being established between them; (ii) interaction between the organic and inorganic components; and (iii) binding of the organic molecules to the surface of the inorganic matrix [1, 2].

Addition of different precursors to a preformed silica network can furnish hybrid materials known as ORMOSILs via the sol–gel methodology. Park et al. [8] have studied silicates modified with alkyl groups, such as methyl, propyl, phenyl, and octyl. Alkoxides have also been used to prepare methylmethoxysilane, dimethoxymethylsilane, and 3-glicidoxypropylmethoxysilane, for example [9–22].

Luminescent nanoparticles constitute sensitive biological tools [23]. Among the nanoparticles that serve as luminescent markers are quantum dots, metal nanoshells, lanthanide oxides and, more recently, hybrid materials containing lanthanide compounds [24–26]. The first systematic study that used the europium(III) ion as a marker dates back to the 1970s [27]. Since then, the spectroscopic properties of lanthanide ions have enabled their use as contrast agents in diagnosis and as probes in immunology (fluoroimmunoassay) [28]. Incorporation of lanthanide compounds into silica nanoparticles yields

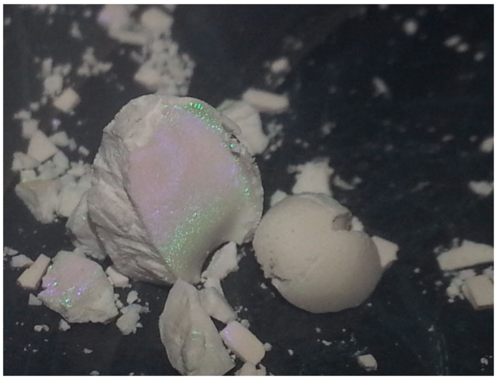

Fig. 1 Photography of the sample prepared with TEOS:DMDMS

attractive materials that can function as luminescent markers—apart from protecting the lanthanide compounds and ensuring that they maintain their properties, the silica matrix confers them with adequate porosity and biocompatibility, allowing them to interact with several kinds of biomolecules [24, 29–31].

Matrix functionalization is a strategy that provides a silica support with novel surface properties, such as hydrophilic or hydrophobic character, and functional groups, which will determine the specific application of the resulting particles. Other features such as particle size, shape, and morphology will also determine the potential uses of the hybrid material. In this context, the present work reports on (i) the preparation of spherical hybrid nanosilicas by means of a modified Stöber methodology, (ii) subsequent doping of the silicas with europium(III) or the europium(III) complex with 1,10-phenanthroline, and (iii) characterization of the final materials by scanning electronic microscopy, thermal analysis, X-ray diffraction, infrared spectroscopy, and photoluminescence.

Experimental

$EuCl_3$ Solution

$EuCl_3$ was prepared after calcination of the corresponding oxide (Eu_2O_3 – Aldrich) at 900 °C, for 2 h, followed by dissolution in HCl 6 mol L^{-1} (Merck). Excess HCl and H_2O were evaporated. Ethanol was subsequently added and evaporated three times. The final concentration of $EuCl_3$ in the ethanolic solution was 0.1 mol L^{-1}.

Europium(III) Complex

The europium (III) complex with 1,10-phenanthroline (phen) was prepared as described in the literature [32]. Under stirring, 200 mg of phen was added to 10.0 mL of ethanol, which was followed by the addition of 2.0 mL of $EuCl_3$ ethanolic solution (0.1 mol L^{-1}). After half an hour, 18.0 mL of acetone was poured into the resulting mixture, to precipitate the complex. The complex was filtered, washed, and dried at 50 °C, for 4 h. The thermogravimetric curve revealed that the complex had molecular formula $[Eu(phen)_2(H_2O)_2]Cl_3$.

Preparation of the Hybrid Silicas

The hybrid silicas were prepared by mixing 1.43 mL of tetraethylorthosilicate (TEOS) with 0.73 mL of methyltrimethoxysilane (MTMS) or 0.73 mL of dimethyldimethoxysilane, (DMDMS), purchased from Aldrich, at a 1:1 M ratio. Then, 15.27 mL of isopropyl alcohol, 2.70 mL of deionized water, and 7.88 mL of ammonium hydroxide were added to the mixture, which was kept under magnetic stirring at 40 °C, for 24 h. The final TEOS:MTMS

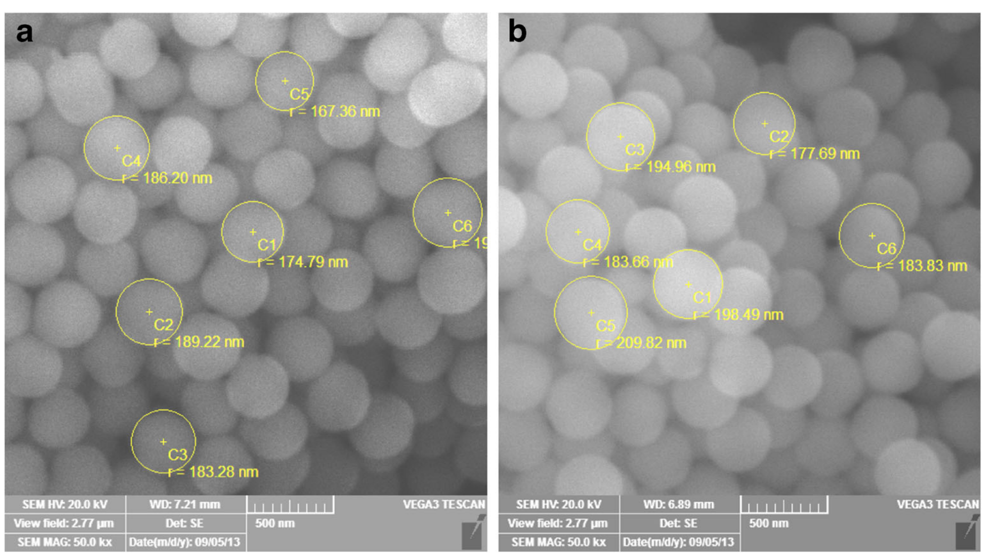

Fig. 2 SEM image of the samples **a** TEOS:DMDMS-APTES-Eu(III)/phen and **b** TEOS:MTMS-APTES-Eu(III)/phen at magnification of 50 kx

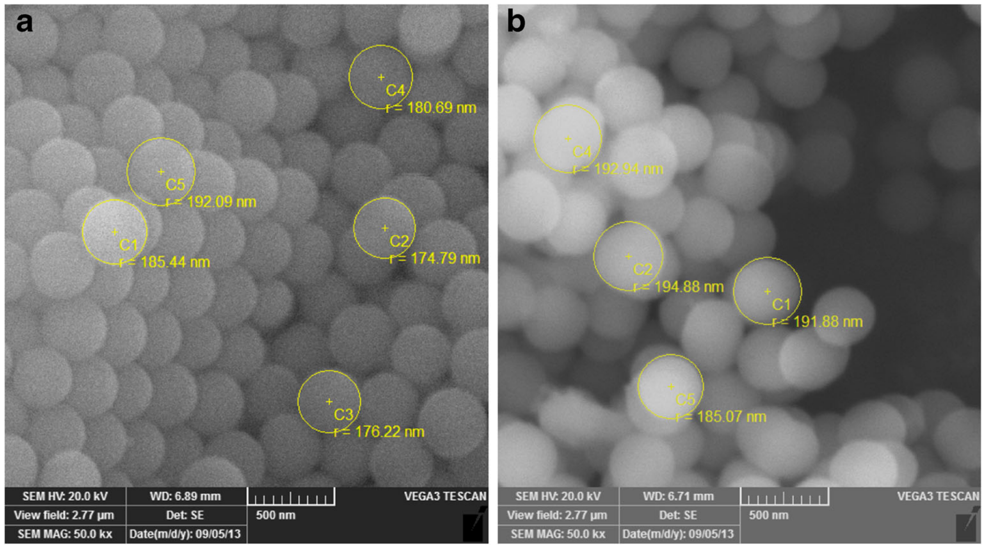

Fig. 3 SEM image of the samples **a** TEOS:DMDMS-APTES-$[Eu(phen)_2(H_2O)_2]Cl_3$ and **b** TEOS:MTMS-APTES-$[Eu(phen)_2(H_2O)_2]Cl_3$ at magnification of 50 kx

and TEOS:DMDMS powders were washed and dried at 60 °C.

Functionalization of the Hybrid Silicas

The hybrid silicas TEOS:MTMS and TEOS:DMDMS were functionalized with 3-aminepropyltriethoxysilane (APTES). To this end, 30.0 mL of toluene was added to 400 mg of dry TEOS:MTMS or TEOS:DMDMS. After 10 min., 2.39 mL of APTES was added to the mixture, which was then kept under magnetic stirring at 80 °C for 24 h. The functionalized TEOS:MTMS-APTES and TEOS:DMDMS-APTES hybrid materials were washed and dried at 60 °C.

Incorporation of the Eu(III) ion and the 1,10-phenanthroline ligand, and of the complex $[Eu(phen)_2(H_2O)_2]Cl_3$ into the functionalized hybrid silicas.

First, the Eu(III) ion and the phen ligand were incorporated into the functionalized hybrid silicas TEOS:MTMS-APTES and TEOS:DMDMS-APTES separately. To this end, 120 mg of TEOS:MTMS-APTES or TEOS:DMDMS-APTES was added to 4.0 mL of ethanol, 1.0 mL of $EuCl_3$ solution (0.1 mol L^{-1}), and 5.0 mL of phen solution (0.1 mol L^{-1}). The mixture was kept under magnetic stirring for 24 h. The final products TEOS:MTMS-APTES-Eu(III)/phen and TEOS:DMDMS-APTES-Eu(III)/phen were washed and dried at 60 °C.

As for incorporation of the complex $[Eu(phen)_2(H_2O)_2]Cl_3$, 50 mg of $[Eu(phen)_2(H_2O)_2]Cl_3$ was dissolved in ethanol, and then 150 mg of TEOS:MTMS-APTES or TEOS:DMDMS-APTES was added to the solution. The mixture was kept under magnetic stirring for 24 h. The final products TEOS:MTMS-APTES-$[Eu(phen)_2(H_2O)_2]Cl_3$ and TEOS:DMDMS-APTES-$[Eu(phen)_2(H_2O)_2]Cl_3$ were washed and dried at 60 °C.

Characterization Techniques

Photoluminescence data were obtained at room temperature, under continuous Xe lamp (450 W) excitation in a Horiba Jobin Yvon Fluorolog-3 spectrofluorimeter equipped with an excitation and emission double monochromator and a photomultiplier R 928 Hammatsu. The emission was collected at 90° from the excitation beam. The slits were placed at 2.0 and 0.5 nm for excitation and emission, respectively; the band pass was 0.5 nm, and the integration time was 0.5 ms. G1227 emission filters were employed (transmittance 100 % for $\lambda > 450$ nm). Decay curves were measured with the aid

Table 1 Percentage of mass loss as a function of the temperature for the samples prepared with DMDMS precursors

Samples	Mass loss up to 200 °C (%)	Mass loss from 200 to 450 °C (%)	Mass loss from 450 to 650 °C (%)
TEOS:DMDMS	8.03	2.59	1.84
TEOS:DMDMS-APTES	7.82	3.29	2.86
TEOS:DMDMS-APTES-Eu(III)/phen	8.12	4.29	3.32
TEOS:DMDMS-APTES-$[Eu(phen)_3(H_2O)_6]Cl_3$	7.34	4.21	2.70

Table 2 Percentage of the mass loss as a function of the temperature for the samples prepared with MTMS precursors

Samples	Mass loss up to 200 °C (%)	Mass loss from 250 to 450 °C (%)	Mass loss from 450 to 650 °C (%)
TEOS:MTMS	7.74	2.74	1.98
TEOS:MTMS-APTES	8.66	3.12	3.57
TEOS:MTMS-APTES-Eu(III)/phen	7.69	4.58	2.66
TEOS:MTMS-APTES-$[Eu(phen)_3(H_2O)_6]Cl_3$	8.47	4.89	3.57

of a phosphorimeter accessory equipped with a Xe Lamp (5 J/Pulse).

Thermal analysis (TG/DTG) was carried out (Thermal Analyst 2100 – TA Instruments SDT 2960 simultaneous DTA-TG) in nitrogen atmosphere at a heating rate of 20 °C $min.^{-1}$, from 25 to 1000 °C.

X-ray diffraction (XRD) was conducted at room temperature using a Rigaku Geigerflex D/max-c diffractometer with monochromated CuKα radiation (λ = 1.54 Å). Diffractoframs were recorded in the 2θ range from 15 to 70° at a resolution of 0.05°.

Infrared absorption spectroscopy (FTIR) was accomplished on a Frontier Perkin Elmer spectrometer; the spectra were acquired in the ATR mode, by scanning the sample 16 times at a resolution of 4 cm^{-1}, from 4000 to 500 cm^{-1}.

Scanning electron microscopy (SEM) was performed on a TESCAN VEGA 3 SBH apparatus.

Results and Discussion

Figure 1 shows the photograph of the hybrid silica sample TEOS:DMDMS before functionalization with APTES. TEOS:MTMS afforded a similar image. Both samples displayed iridescence. This phenomenon commonly occurs in opals, white stones consisting of silica microspheres in which the diameter of the particles is similar to the wavelength of visible light. This arrangement diffracts light and makes the material iridescent. The photograph in Fig. 1 also revealed that the spherical particles had homogeneous size.

Figure 2 depicts the scanning electron micrographs of the TEOS:DMDMS and TEOS:MTMS samples after functionalization with APTES and incorporation of Eu(III)/phen. The spherical silica particles had homogeneous size distribution and were polydispersed. The mean diameter of the particles in the TEOS:DMDMS-APTES-Eu(III)/phen and TEOS:MTMS-APTES-Eu(III)/phen samples was 180 and 190 nm, respectively.

Figure 3 illustrates the micrograph of the samples obtained after TEOS:MTMS and TEOS:DMDMS functionalization with APTES and incorporation of the complex $[Eu(phen)_2(H_2O)_2]Cl_3$.

Figures 2 and 3 demonstrated that particle morphology was the same irrespective of the incorporation of individual Eu(III) ions and phen ligands or of the complex $[Eu(phen)_2(H_2O)_2]Cl_3$ into the functionalized hybrid silicas.

Thermal analysis helped to identify the presence of organic groups in the silica (Tables 1 and 2).

All the samples underwent three mass loss steps. Up to 200 °C, the average mass loss was 8 % and it corresponded to loss of the solvent used during preparation of the hybrid silicas and/or incorporation of Eu(III) and phen or the complex $[Eu(phen)_3(H_2O)_6]Cl_3$. The second step occurred between 200 and 450 °C and referred to the organic component of the hybrid materials. On going from TEOS:DMDMS(or MTMS) to TEOS:DMDMS(or MTMS)-APTES-$[Eu(phen)_3(H_2O)_6]Cl_3$, mass loss increased, which was consistent with the larger organic content in the latter samples. The third mass loss was associated with residual carbon and dehydroxylation. Together, the results indicated functionalization of TEOS:DMDMS (or MTMS) with APTES as well as incorporation of Eu(III)/phen or the complex $[Eu(phen)_3(H_2O)_6]Cl_3$.

The X-ray diffraction patterns of all the samples displayed a large halo between 2θ = 10 to 30° (very broad peak at 23.5°), which confirmed their amorphous structure [19, 33, 34].

As for infrared spectroscopy, the bands relative to -OH stretching appeared at 3653 and 3432 cm^{-1}, which suggested incomplete condensation of the precursors [35]. The bands due to CH stretching of the methyl groups of the precursors

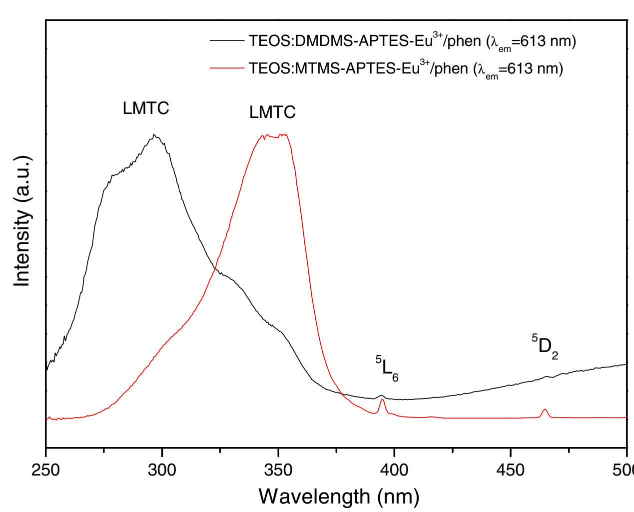

Fig. 4 Excitation spectra of TEOS:DMDMS-APTES-Eu(III)/phen and TEOS:MTMS-APTES-Eu(III)/phen

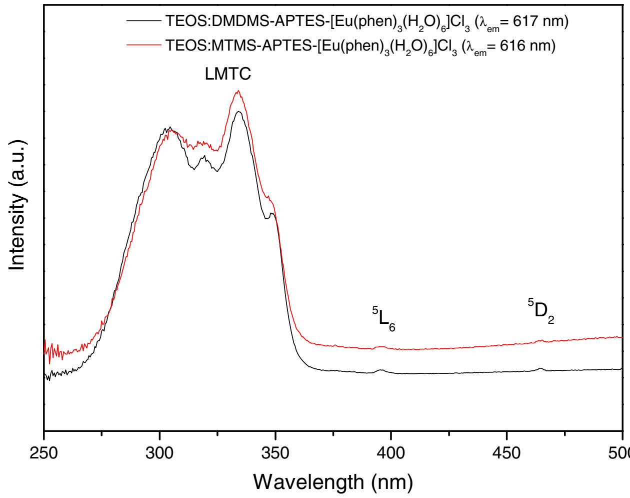

Fig. 5 Excitation spectra of TEOS:DMDMS-APTES-[Eu(phen)$_3$(H$_2$O)$_6$]Cl$_3$and TEOS:MTMS-APTES-[Eu(phen)$_3$(H$_2$O)$_6$]Cl$_3$

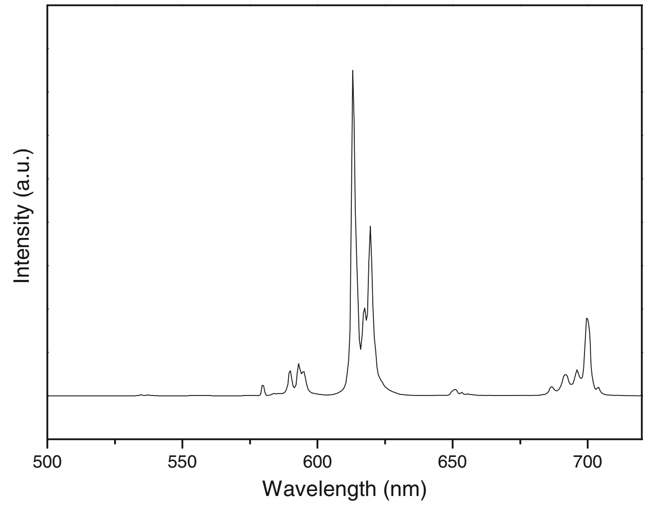

Fig. 7 Emission spectrum of the complex [Eu(phen)$_2$(H$_2$O)$_2$]Cl$_3$, excited at the LMCT band (340 nm)

MTMS and DMDMS emerged at 2990 and 2900 cm^{-1} [19, 36]. The intense broad band at 1102 cm^{-1} corresponded to asymmetric stretching vibrations of Si-O-Si. The band associated with the bending mode of Si-O-Si arose at 475 cm^{-1} [28] and indicated formation of a dense silica network [37–39]. The ratio between the bands corresponding to Si-O-Si and Si-OH bending, at 1102 and 952 cm^{-1}, respectively, decreased, which confirmed functionalization of the hybrid silicas with APTES and incorporation of the europium(III) complex.

Figures 4 and 5 depict the excitation spectra of TEOS:DMDMS(or MTMS)-Eu(III)/phen and TEOS:DMDMS(or MTMS)-APTES-[Eu(phen)$_3$(H$_2$O)$_6$]Cl$_3$, respectively.

According to Fig. 4, the large band was due to Ligand-Metal Charge Transfer (LMCT). The sample TEOS:MTMS-APTES-Eu(III)/phen displayed maximum excitation at 351 nm, in agreement with the literature [40–42]. As for TEOS:DMDMS-APTES-Eu(III)/phen, the maximum appeared at 290 nm, which has also been observed in the literature [35].

On the basis of Fig. 5, TEOS:DMDMS-APTES-[Eu(phen)$_3$(H$_2$O)$_6$]Cl$_3$ and TEOS:MTMS-APTES-[Eu(phen)$_3$(H$_2$O)$_6$]Cl$_3$ presented similar spectral profiles. The large band between 250 and 370 nm with maximum at 334 nm referred to the phen ligand.

The 4f - 4f excitation lines of the Eu(III) ion ($^7F_0 \rightarrow {}^5L_6$ e $^7F_0 \rightarrow {}^5D_2$) appeared in all the spectra shown in Figs. 4 and 5, but they were less intense than the LMCT band. Therefore, an efficient sensitization process took place between the ligand and the ion [42].

Figure 6 brings the emission spectra of TEOS:DMDMS-APTES-Eu(III)/phen and TEOS:MTMS-APTES-Eu(III)/phen.

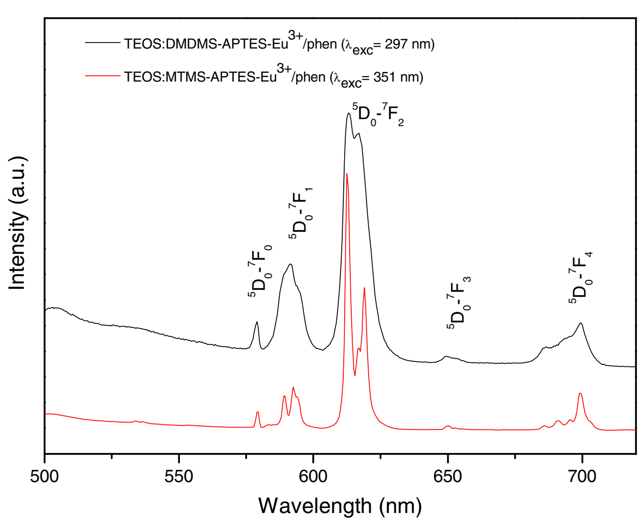

Fig. 6 Emission spectra of TEOS:DMDMS-APTES-Eu(III)/phen and TEOS:MTMS-APTES-Eu(III)/phen

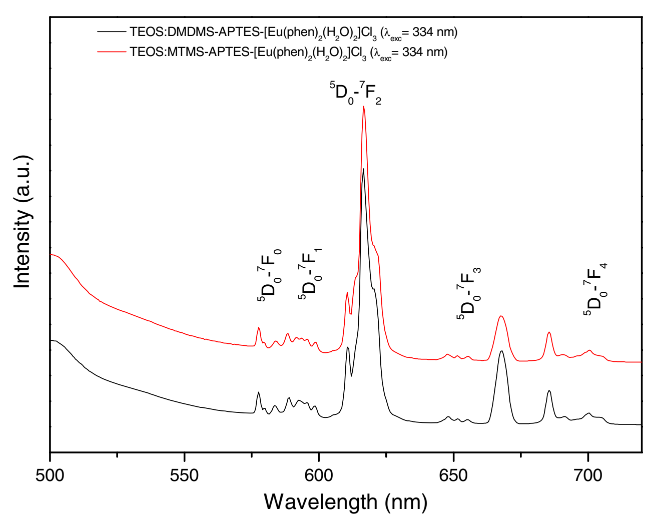

Fig. 8 Emission spectra of TEOS:DMDMS-APTES-[Eu(phen)$_3$(H$_2$O)$_6$]Cl$_3$ and TEOS:MTMS-APTES-[Eu(phen)$_3$(H$_2$O)$_6$]Cl$_3$

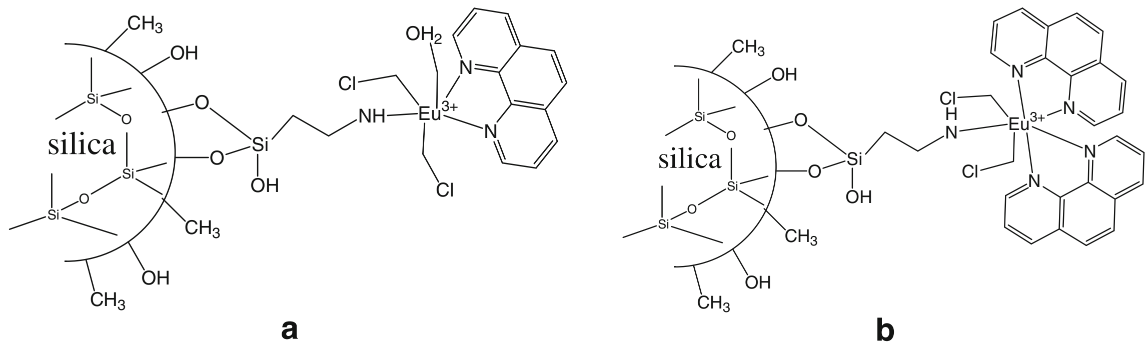

Fig. 9 Possible structures of TEOS:DMDMS(or MTMS)-APTES-[Eu(phen)$_3$(H$_2$O)$_6$]Cl$_3$

TEOS:DMDMS-APTES-Eu(III)/phen and TEOS:MTMS-APTES-Eu(III)/phen exhibited similar spectral profiles upon excitation at the corresponding LMCT band, 297 and 351 nm, respectively, but the band definitions were different. The characteristic emission bands corresponded to transition from the excited state $^5D_0$ to the fundamental level $^7F_{0,\ 1,\ 2,\ 3,\ and\ 4}$. The transition between non-degenerate levels $^5D_0 \rightarrow {}^7F_0$ appeared in both spectra, which indicated that the Eu(III) ion occupied a site without inversion center [43].

Figure 7 corresponds to the emission spectrum of the complex ([Eu(phen)$_2$(H$_2$O)$_2$]Cl$_3$).

Comparison of the emission spectra in Figs. 6 and 7 showed that the spectrum of TEOS:MTMS-APTES-Eu(III)/phen was identical to that of the free complex [Eu(phen)$_2$(H$_2$O)$_2$]Cl$_3$, indicating that this complex may have arisen on the hybrid silica surface. The larger and less defined bands verified for TEOS:DMDMS-APTES-Eu(III)/phen might have originated from a distorted symmetry site in the Eu(III)$^{3+}$ ion. The emission spectrum suggested that a complex emerged on the silica surface, but its interaction with APTES was not evident.

Figure 8 presents the emission spectra of TEOS:DMDMS-APTES-[Eu(phen)$_3$(H$_2$O)$_6$]Cl$_3$ and TEOS:MTMS-APTES-[Eu(phen)$_3$(H$_2$O)$_6$]Cl$_3$.

The spectral profiles of TEOS:DMDMS-APTES-[Eu(phen)$_3$(H$_2$O)$_6$]Cl$_3$ and TEOS:MTMS-APTES-[Eu(phen)$_3$(H$_2$O)$_6$]Cl$_3$ were identical, but they differed from the spectrum of the free complex [Eu(phen)$_3$(H$_2$O)$_6$]Cl$_3$ (Fig. 7). The band relative to the transition $^5D_0 \rightarrow {}^7F_0$ presented a shoulder, indicating that the Eu(III) ion had more than one symmetry site. The transition $^5D_0 \rightarrow {}^7F_1$ gave rise to more than three bands, suggesting that the crystalline field could be 2 J + 1 [44], ascribed to the presence of distinct symmetry sites. The structure of the Eu(III) complex incorporated into the hybrid silicas, represented in Fig. 9a, b, could account for this profile. The differences in the emission spectra of TEOS:DMDMS-APTES-[Eu(phen)$_3$(H$_2$O)$_6$]Cl$_3$ and TEOS:MTMS-APTES-[Eu(phen)$_3$(H$_2$O)$_6$]Cl$_3$ could indicate interaction between [Eu(phen)$_3$(H$_2$O)$_6$]Cl$_3$ and APTES.

Table 3 lists I($^5D_0 \rightarrow {}^7F_2$)/I($^5D_0 \rightarrow {}^7F_1$) Intensity Ratios, Experimental Judd-Ofelt Intensity Parameters ($\Omega_{2\ and\ 4}$), the Radiative and Nonradiative Decay Rates (A_{rad}, A_{nrad}), the Experimental Lifetime (τ), and the Quantum Efficiency (η) of the Eu(III) ion in the different materials, as calculated from the emission spectrum with the aid of the LUMPAC Lanthanide Luminescence Software [45]. The theory is well discussed in the literature [46, 47].

The Judd-Ofelt parameters provide information about the Eu(III) ion surroundings. Large Ω_2 values indicate high hypersensitivity of the transition $^5D_0 \rightarrow {}^7F_2$ and the covalent chemical bond [48–50]. The Ω_4 parameters correspond to the rigidity of the network and are under the influence of the vibronic transitions of the Eu(III) ion-ligand bond [51]. The Ω_2 and Ω_4 values obtained for the Eu(III) ion incorporated into the hybrid silicas differed from those achieved for the free complex [Eu(phen)$_3$(H$_2$O)$_6$]Cl$_3$ (Table 3). TEOS:DMDMS-APTES-Eu^{3+}/phen had smaller Ω_2, due to the influence of its surroundings. Indeed, the emission spectrum of this sample

Table 3 I($^5D_0 \rightarrow {}^7F_2$)/I($^5D_0 \rightarrow {}^7F_1$) intensity ratios, experimental Judd-Ofelt intensity ($\Omega_{2\ and\ 4}$), radiative emission rates (A_{rad}), nonradiative decay rates (A_{nrad}), experimental lifetime (τ), and quantum efficiency (η)

Samples	0–2/0–1	Ω_2 10^{-20} (cm^2)	Ω_4 10^{-20} (cm^2)	A_{rad} (s^{-1})	A_{nrad} (s^{-1})	$\tau_{exp.\ (ms)}$	η (%)
TEOS:DMDMS-APTES-Eu^{3+}/phen	2.50	4.42	2.16	214.57	3356.86	0.280	6.01
TEOS:MTMS-APTES-Eu^{3+}/phen	4.16	8.14	3.20	341.24	2039.71	0.420	14.33
TEOS:DMDMS-APTES-[Eu(phen)$_2$(H$_2$O)$_2$]Cl$_3$	5.20	9.19	2.76	365.98	2967.35	0.300	10.98
TEOS:MTMS-APTES-[Eu(phen)$_2$(H$_2$O)$_2$]Cl$_3$	4.54	8.02	2.31	324.62	3521.53	0.260	8.44
[Eu(phen)$_2$(H$_2$O)$_2$]Cl$_3$	7.57	13.37	9.26	586.34	1739.24	0.430	25.21

(Fig. 6) had evidenced that Eu^{3+}/phen remained on the silica surface, so the -CH_3 and -OH groups of TEOS:DMDMS could alter the surroundings of Eu(III). These results reflected in the smaller A_{rad} (214.57 s^{-1}), lifetime (0.28 ms), and quantum efficiency (6.01 %), and higher A_{nrad} (3356.86 s^{-1}).

TEOS:MTMS-APTES-Eu(III)/phen, TEOS:DMDMS-APTES-$[Eu(phen)_3(H_2O)_6]Cl_3$, and TEOS:MTMS-APTES-$[Eu(phen)_3(H_2O)_6]Cl_3$ displayed similar $\Omega_{2\ and\ 4}$, albeit lower than those of the free complex $[Eu(phen)_3(H_2O)_6]Cl_3$. Hence, the hybrid silica surface affected the Eu(III) ion emission. The A_{rad}, A_{nrad}, and τ parameters can furnish information about the population of the excited state and the competitive nonradiative and radiative decay processes [52].

Conclusion

By means of the sol–gel methodology, it is possible to obtain luminescent silica nanoparticles with controlled size and morphology, for potential application as drug delivery systems and luminescent markers. If the lanthanide complex originates on the silica surface, the quantum efficiency decreases. However, compared with the free lanthanide complex, the complex incorporated into hybrid silica is advantageous, because the doping level was low— 1 %. The silica surface can influence the luminescent properties of the lanthanide ion and determine the application of the resulting material, because the resulting nanoparticle can be either hydrophobic or hydrophilic.

Acknowledgments The authors acknowledge the Brazilian research funding agencies CNPq, CAPES, and (grant 2011/15199–1 C.B.A; 2011/09823–4 and 2012/11673–3 E.J.N.) São Paulo Research Foundation (FAPESP).

References

1. Sanchez C, Boissiere C, Cassaignon S, Chaneac C, Durupthy O, Faustini M, Grosso D, Laberty-Robert C, Nicole L, Portehault D, Ribot F, Rozes L, Sassoye C (2013) Molecular engineering of funtional inorganic and hybrid materials. Chem Mater 1–20
2. José NM, Prado LASA (2005) Materiais Híbridos Orgânicos-Inorgânicos: preparação e Algumas Aplicações. Quim Nova 28: 281–288
3. Sanchez C, Bellevillec P, Popalld M, Nicoleab L (2011) Applications of advanced hybrid organic–inorganic nanomaterials: from laboratory to market. Chem Soc Rev 40:696–753
4. Sanchez C, Rozes L, Ribot F, Laberty-Robert C, Grosso D, Sassoye C, Boissiere C, Nicole L (2010) Chimie douce: a land of opportunities for the designed construction of functional inorganic and hybrid organic–inorganic nanomaterials. C R Chim 13:3–39
5. Schimidt H, Krug H (1994) Sol–gel based inorganic–organic composites materials In: Neilsen PW, Allcok HR, Wynne KJ (Ed.). Inorganic and organometallic polymers II. Washington, D. C.: American Chemical Society 15:183–194.
6. Sanchez C, Julian B, Belleville P, Popall M (2005) Applications of hybrid organic–inorganic nanocomposites. J Mater Chem 15:3559–3592
7. Sanchez C, François R (1994) Design of hybrid organic–inorganic materials synthesized via solgel chemistry. New J Chem 18:1007–1047
8. Park M, Komarneni S (1998) Effect of substituted alkyl groups on textural properties of ORMOSILs. J Mater Sci 33:3817–3821
9. del Monte F, Cheben P, Grover CP, Mackenzie JD. (1999) Preparation and Optical Characterization of Thick-Film Zirconia and Titania Ormosils. J Sol–Gel Sci Technol. 15:73–85.
10. Altman JC, Stone RE, Dunn B, Nishida F (1991) Solid-state laser using a Rhodamine-doped silica-gel compound. IEEE Photon Technol Lett 3:189–190
11. Wojcik AB, Klein LC (1995) Transparent Inorganic/Organic Copolymers by the Sol–Gel Process: Copolymers of Tetraethyl Orthosilicate (TEOS), Vinyl Triethoxysilane (VTES) and (Meth)acrylate Monomers. J Sol–Gel Sci Technol 4:57–66
12. Reisfeld R, Gvishi R, Burshtein Z (1995) Photostability and loss mechanism of solid-state red perylimide dye lasers. J Sol–Gel Sci Technol 4:49–55
13. Gvishi R (2009) Fast sol–gel technology: from fabrication to applications. J Sol–Gel Sci Technol 50:241–253
14. Gupta R, Chaudhury NK (2007) Entrapment of biomolecules in sol–gel matrix for applications in biosensors: Problems and future prospects. Biosens Bioelectron 22:2387–2399
15. Ibrahima WAW, Veloo KV, Sanagia MM (2012) Novel sol–gel hybrid methyltrimethoxysilane–tetraethoxysilane as solid phase extraction sorbent for organophosphorus pesticides. J. Chromatogr A 1229: 55–62
16. Nadargi DY, Kalesh RR, Rao AV (2009) Rapid reduction in gelation time and impregnation of hydrophobic property in the tetraethoxysilane (TEOS) based silica aerogels using NH_4F catalyzed single step sol–gel process. J Alloys Compd 480:689–695
17. Gvishi R, Strum G, Shitrit N, Dror R (2008) Optical waveguide fabrication using a fast sol–gel method. Opt Mater 30:1755–1758
18. Morpurgo M, Teoli D, Palazzo B, Bergamin E, Realdon N, Guglielmi M (2005) Influence of synthesis and processing conditions on the release behavior and stability of sol–gel derived silica xerogels embedded with bioactive compounds. Il Farmaco 60:675–683
19. Azevedo CB, Souza EA, Faria EH, Rocha LA, Calefi PS, Ciuffi KJ, Nassar EJ (2013) Optical properties of Eu-doped hybrid materials prepared from dimethyl and methyl alkoxides precursors. J Lumin 134:551–557
20. Avila LR, Nassor ECO, Pereira PFS, Cestari A, Ciuffi KJ, Calefi PS, Nassar EJ (2008) Preparation and properties of europium-doped phosphosilicate glasses obtained by the sol–gel method. J Non-Cryst Solids 354:4806–4810
21. Nassor ECO, Ávila LR, Pereira PFS, Ciuffi KJ, Calefi PS, Nassar EJ (2011) Influence of the hydrolysis and condensation time on the preparation of hybrid materials. Mater Res 14:1–6
22. Nassar EJ, Messaddeq Y, Ribeiro SJL (2002) Influência da catálise ácida e básica na preparação da sílica funcionalizada pelo método sol–gel. Quim Nova 25:27–31
23. Pei X, Zhang B, Tang J, Liu B, Lai W, Tang D (2013) Sandwich-type immunosensors and immunoassays exploiting nanostructure labels: a review. Anal Chim Acta 758:1–18
24. Knopp D, Tang D, Niessner R (2009) Review: bioanalytical applications of biomolecule-functionalized nanometer-sized doped silica particles. Anal Chim Acta 647:14–30
25. Cháfer-Pericás C, Maquieira A, Puchades R (2012) Functionalized inorganic nanoparticles used as labels in solid-phase immunoassays. Trends Anal Chem 31:144–156
26. Cummins CM, Koivunen ME, Stephanian A, Geeb SJ, Hammock BD, Kennedy IM (2006) Application of europium(III) chelate-dyed

nanoparticle labels in a competitive atrazine fluoroimmunoassay on an ITO waveguide. Biosens Bioelectron 21:1077–1085
27. Diamandis EP (1988) Immunoassays with time-resolved fluorescence spectroscopy: principles and applications. Clin Biochem 21:139–150
28. Martins TS, Isolani PC (2005) Terras raras: aplicações industriais e biológicas. Quim Nova 28:111–117
29. Wu X, Wu M, Zhao JX (2013) Recent development of silica nanoparticles as delivery vectors for cancer imaging and therapy. Nanotechnology, Biology, and Medicine, Nanomedicine. doi:10.1016/j.nano.2013.08.008
30. Lourenço AVS, Kodaira CA, Ramos-Sanchez EM, Felinto MCFC, Goto H, Gidlund M, Malta OL, Brito HF (2013) Luminescent material based on the $[Eu(TTA)_3(H_2O)_2]$ complex incorporated into modified silica particles for biological applications. J Inorg Biochem 123:11–17
31. Bitar A, Ahmad NM, Fessi H, Elaissari A (2012) Silica-based nanoparticles for biomedical applications. Drug Discov Today 17:1147–1154
32. Sousa FJ, de Lima GPA, Pereira PFS, Ávila LR, Ciuffi KJ, Nassar EJ, Calefi PS (2010) Incorporation of luminescent complex into nanoparticles and films obtained by the sol–gel methodology. Mater Res 13:71–75
33. Ribeiro TJ, de Lima OJ, de Faria EH, Rocha LA, Calefi PS, Ciuffi KJ, Nassar EJ (2014) Calcium phosphate as precursors of hydroxyapatite. An Acad Bras Cienc 86:217–226
34. Al-Harbi T, Al-Hazmi F, Mahmoud WE (2012) Synthesis and characterization of nanoporous silica film via non-surfactant template sol–gel technique. Superlattice Microst 52:643–647
35. Wang X-D, Shen Z-X, Sang T, Cheng X-B, Li M-F, Chen L-Y, Wang Z-S (2010) Preparation of spherical silica particles by Stöber process with high concentration of tetra-ethyl-orthosilicate. J Colloid Interface Sci 341:23–29
36. Takeda Y, Komori Y, Yoshitake H (2013) Direct Stöber synthesis of monodisperse silica particles functionalized with mercapto-, vinyl- and aminopropylsilanes in alcohol–water mixed solvents. Colloids Surf A Physicochem Eng Asp 422:68–74
37. Bertoluzza A, Fagnano C, Morelli MA, Gottardi V, Guglielmi M (1982) Raman and infrared spectra on silical-gel evolving toward glass. J Non-Cryst Solids 48:117–128
38. Duran A, Navarro JMF, Casariego P, Joglar A (1986) Structural considerations about SiO_2 glasses prepared by sol–gel. J Non-Cryst Solids 82:69–77
39. Nassar EJ, Neri CR, Calefi PS, Serra OA (1999) Functionalized silica sinthesized by sol–gel process. J Non-Cryst Solids 247:124–128
40. Sheng K, Yan B (2009) Coordination bonding assembly and photophysical properties of Europium organic/inorganic/polymeric hybrid materials. J Photochem Photobiol A Chem 206:140–147
41. Liu D, Shi Q, Wang Z (2012) Color-tunable heat-resistant polyaryletherketones co-coordinated with various rare earth ions. Opt Mater 34:1815–1821
42. Cunjin X (2010) Photophysical properties of a new ternary europium complex with 2-thenoyltrifluoroacetone and 5-nitro-1,10-phenanthroline. J Rare Earths 28:854–857
43. Serra OA, Nassar EJ, Zapparolli G, Rosa ILV (1994) Organic complexes of Eu III supported in functionalyzed silica gel: highly luminescent materials. J Alloys Compd 207–208:454–456
44. Matos MG, de Faria EH, Rocha LA, Calefi PS, Ciuffi KJ, Nassar EJ, Sarmento VHV (2014) Synthesis and photoluminescent properties of yttrium vanadate phosphor prepared by the non-hydrolytic sol–gel process. J Lumin 147:190–195
45. Dutra JDL, Bispo TD, Freire RO (2014) LUMPAC Lanthanide Luminescence Software: efficient and user friendly. J Comput Chem 35:772–775
46. Mesquita ME, Silva FRG, Albuquerque RQ, Freire RO, Conceição EC, da Silva JEC, Júnior NBC, Sá GF (2004) Eu(III) and Gd(III) complexes with pirazyne-2-carboxylic acid: luminescence and modelling of the structure and energy transfer process. J Alloys Compd 366:124–131
47. Souza AP, Rodrigues LCV, Brito HF, Alves Jr S, Malta OL (2010) Photoluminescence study of new lanthanide complexes with benzene seleninic acids. J Lumin 130:181–189
48. da Silva AA, Davolos MR (2011) Determination of the local site occupancy of Eu^{3+} ions in $ZnAl_2O_4$ nanocrystalline powders. Opt Mater 33:1226–1233
49. Jorgensen CK, Reisfeld R (1983) Judd-Ofelt parameters and chemical bonding. J Less-Common Met 93:107–112
50. Nassar EJ, Pereira PFS, de Oliveira Nassor EC, Ávila LR, Ciuffi KJ, Calefi PS (2007) Nonhydrolytic sol–gel synthesis and characterization of YAG. J Mater Sci 42:2244–2249
51. Babu AB, Jamalaiah BC, Suhasini T, Rao TS, Moorthy LR (2011) Optical properties of Eu^{3+} ions in lead tungstate tellurite glasses. Solid State Sci 13:574–578
52. Lima PP, Malta OL, Alves Jr S (2005) Estudo Espectroscópico de Complexos de Eu^{3+}, Tb^{3+} e Gd^{3+} com Ligantes Derivados de Ácidos Dipicolínicos. Quim Nova 28:805–808